



Short Communication

Molecular structure on the detoxification of fluorinated liquid crystal monomers with reactive oxidation species in the photocatalytic process



Shaoxiong He, Mingjie Shen, Enya Wu, Renli Yin, Mingshan Zhu*, Lixi Zeng

Guangdong Key Laboratory of Environmental Pollution and Health, School of Environment, Guangdong-Hongkong-Macau Joint Laboratory of Collaborative Innovation for Environmental Quality, Jinan University, Guangzhou, 511443, China

ARTICLE INFO

Article history:

Received 18 October 2021

Received in revised form

7 December 2021

Accepted 8 December 2021

Keywords:

Fluorinated liquid crystal monomers

Structure-reactivity relationships

Photocatalytic process

Electrostatic potential distribution

Detoxification

ABSTRACT

Fluorinated liquid crystal monomers (LCMs) are begun to emerge as new persistent organic pollutants. Herein, the structure-reactivity relationships of fluorinated LCMs 1,2,3-trifluoro-5-[3-(3-propylcyclohexyl)cyclohexyl]benzene (TPrCB), 1,2-difluoro-4-[*trans*-4-(*trans*-4-propylcyclohexyl)cyclohexyl]benzene (DPrCB), 4-[(*trans,trans*-4'-(3-Buten-1-yl)[1,1'-bicyclohexyl]-4-yl]-1,2-difluoro-benzene (BBDB) and 1-[4-(4-ethylcyclohexyl)cyclohexyl]-4(trifluoromethoxy)benzene (ECTB) subject to photocatalysis-generated oxidation species were investigated. The degradation rate constant of BBDB was 3.0, 2.6, and 6.8 times higher than DPrCB, TPrCB and ECTB, respectively. The results reveal that BBDB, DPrCB and TPrCB had mainly negative electrostatic potential (ESP) regions which were vulnerable to electrophilic attack by h^+ , $\bullet OH$ and $\bullet O_2^-$, while ECTB was composed of mainly positive ESP regions which were vulnerable to nucleophilic attack by $\bullet OH$ and $\bullet O_2^-$. The detoxification processes of BBDB, DPrCB and TPrCB included carbon bond cleavage and benzene ring opening. However, the methoxy group of ECTB reduced the nucleophilic reactivity on the benzene ring, leading to slower detoxification efficiency. These findings may help to develop LCMs treatment technologies based on structure-reactivity relationships. © 2021 The Author(s). Published by Elsevier B.V. on behalf of Chinese Society for Environmental Sciences, Harbin Institute of Technology, Chinese Research Academy of Environmental Sciences. This is an open access article under the CC BY-NC-ND license (<http://creativecommons.org/licenses/by-nc-nd/4.0/>).

1. Introduction

Liquid crystal displays (LCDs), an essential part of most electronic products, have been increasingly produced worldwide due to the ever growing demand [1]. The global LCD shipment reached 198 million m^2 in 2018, introducing numerous scrapped electronic waste around the world [2,3]. The chemicals in LCDs are mainly composed of liquid crystal monomers (LCMs), the existence and impact of which in the environment have only recently begun to attract attention and be publicly reported [4]. Su et al. (2019) recently reported that exposure to LCMs led to adverse health effects and pointed out that about a quarter of the LCMs were identified as persistent and bioaccumulative (P&B) chemicals [2,5,6]. Generally, LCMs are less likely to combine with other basic materials in LCD devices and may have strong environmental persistence as well as mobility [7]. Thus, LCMs may easily enter and

remain in the water, atmosphere, soil and other environmental media during the use, recycling and disposal of LCD devices, which can cause a serious threat to human health and the environment [8].

LCMs generally contains benzene or diphenyl skeleton structures with several functional groups, such as cyano, fluorine, chlorine and bromine. It is known that the differences in functional groups in organic pollutants may lead to their completely different detoxification processes [9–11]. For example, five or six membered substituents on sulfonamides (SAs) were confirmed to change the molecular orbital distribution and stability, thus leading to different degradation efficiencies of SAs [10]. Furthermore, the category and position of functional groups in the molecular structure may play important roles in guiding the degradation mechanisms and pathways [12–14]. For instance, the degradation mechanisms of three N-chloro- α -amino acids were investigated, and the electron-donating groups (EDG) substituted on the N-terminal were found to promote both concerted Grob fragmentation (CGF) and β -elimination (β -E) processes, while EDG and electron-withdrawing groups on the α -carbon were determined to conduct the CGF and

* Corresponding author.

E-mail address: zhumingshan@jnu.edu.cn (M. Zhu).

β -E processes, respectively [12]. Therefore, we hypothesize that the degradation mechanisms and detoxification processes of LCMs with similar molecular structures may be dependent on their unique structures and functional groups, which have not yet been reported.

As emerging persistent organic pollutants (POPs), LCMs have stable chemical structures, which require highly oxidative species to accelerate their mineralization. Photocatalytic oxidation technology has been known as an efficient approach for the decomposition of organic pollutants by using the photocatalysis-generated reactive oxidation species (ROS, viz. h^+ , $\bullet OH$ and $\bullet O_2^-$) [15–20]. In our previous study, 46 LCMs in e-waste dust samples were investigated by a dedicated target analysis, through which the detection frequency of 1,2,3-trifluoro-5-[3-(3-propylcyclohexyl)cyclohexyl]benzene (TPrCB) was found to be 100% in LCD and non-LCD dismantling lines with concentrations of 8.83–190,000 and 8.23–496 $ng\ g^{-1}$, respectively [21]. These results demonstrated that TPrCB was a fluorinated LCM that exists widely in the environment. Based on this, TPrCB with other structure-similar fluorinated LCMs, including 1,2-difluoro-4-[*trans*-4-(*trans*-4-propylcyclohexyl)cyclohexyl]benzene (DPrCB), 4-[(*trans*,*trans*-4'-(3-Buten-1-yl)[1,1'-bicyclohexyl]-4-yl]-1,2-difluoro-benzene (BBDB) and 1-[4-(4-ethylcyclohexyl)cyclohexyl]-4(trifluoromethoxy)benzene (ECTB) were selected as targets to investigate the structure-reactivity relationships of the detoxification processes of LCMs and ROS. Commercial TiO_2 (Degussa P25) was used as the photocatalyst and four representative fluorinated LCMs as the targets. The main objectives of this study were to investigate: (i) the degradation efficiency and defluorination extent of the fluorinated LCMs during the photocatalytic process, (ii) the relationship between molecular structure and degradation efficiency, and (iii) degradation pathways of the fluorinated LCMs and toxicity assessment of the intermediates. For the first time, the experimental and theoretical reports of LCMs' detoxification processes in a photocatalytic system are provided. This study is expected to expand our understanding of the degradation mechanism and detoxification process of LCMs under the influence of their unique functional groups.

2. Materials and methods

2.1. Photocatalytic experiments

The photocatalytic processes of LCMs (1, 5, 10 and 20 $mg\ L^{-1}$) by P25 (0.6 $g\ L^{-1}$) were evaluated under simulated sunlight from a 300 W Xenon light source (PLS-SXE300D, Beijing Perfectlight Technology Co., Ltd., China) with a light intensity of 150 $mW\ cm^{-2}$ in a 100 mL magnetically stirred quartz reactor. The LCMs were dissolved in 50 vol% acetonitrile water, which was made from a mixed solution of 50 mL acetonitrile and 50 mL ultra-pure water. Acetonitrile was used as solubilizer to dissolve LCMs in water. The samples (1 mL) of the reaction solutions were taken at a given time interval and filtered with a 0.22 μm filter membrane, followed by analysis with high-performance liquid chromatography (HPLC, Shimadzu, LC-16, Japan). The degradation ratios of LCMs during the photocatalytic process were calculated by the ratio of the peak area of the chromatogram at a given time to the peak area of the original sample.

2.2. Computational methods

The density functional theory (DFT) calculation was performed by Gaussian at the B3LYP/6–31 + G** level [22], which is beneficial to predict the reactive sites and identify the degradation pathways

[23,24]. Electrostatic potential (ESP) distributions and average local ionization energy (ALIE) distributions on the van der Waals (vdW) surface (electron density isosurfaces of 0.01 a.u.) were run and graphed with the Multiwfn and GaussView software, which help to predict and locate the sites for electrophilic and nucleophilic reactions [25]. Generally, the negative ESP regions are associated with electrophilic reactivity and the positive ones are linked to nucleophilic reactivity [26,27]. In the negative ESP regions, the smaller ALIE value represents the weaker electron binding as well as the higher average energy of electrons. Thus, the negative ESP areas with smaller ALIE values are more prone to electrophilic reactions. Moreover, given that the P25/photocatalytic system contains free radicals and non-radical attacks, a dual descriptor (DD) defined was introduced to characterize both nucleophilicity and electrophilicity oxidation [28,29]. The value of the Fukui function is proportional to the reactivity of the molecular sites. The DD value per atom A in the molecule is defined as:

$$f_A^{(2)} = f_A^+ - f_A^- = 2q_A(N) - q_A(N-1) - q_A(N+1) \quad (1)$$

where is the DD value of atom A, while is the electron population of atom A.

3. Results and discussion

3.1. Different reaction kinetics of the fluorinated LCMs

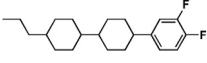
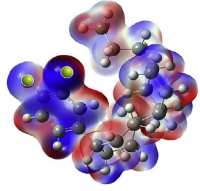
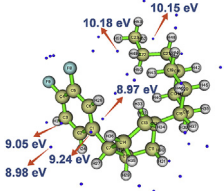
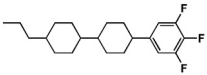
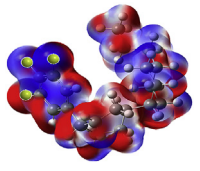
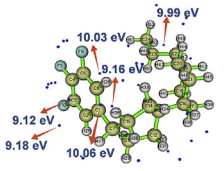
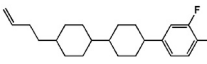
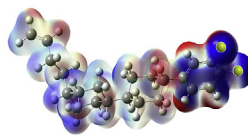
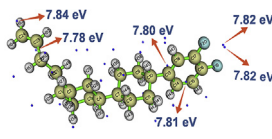
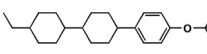
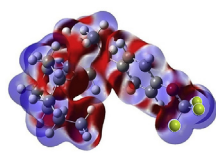
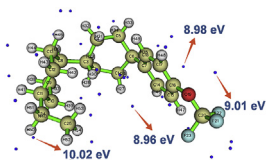
The scanning electron microscope (SEM) (Fig. S1a) and transmission electron microscopes (TEM) (Fig. S1b) images show that the particle size of the commercial P25 ranges from 20 to 50 nm. Given that TPrCB is widespread in the environment, photocatalytic experiments of TPrCB with series concentrations were conducted (Fig. S2a). The photodegradation rates of TPrCB in various natural water were shown in Fig. S2b and the characteristics of the natural water were shown in Table S1. Due to the competition of organic impurities, the photodegradation rate of TPrCB was slightly inhibited in river water and tap water. As shown in Table 1, the structures of the four fluorinated LCMs are mainly composed of benzene ring and cyclohexane, while a unique methoxy group is connected to the benzene ring in ECTB. There was no obvious difference in the photodegradation rates of TPrCB and DPrCB, while the reactions of BBDB and ECTB were significantly different (Fig. 1a). Note that the separate P25 adsorption (30 min) and simulated sunlight irradiation (Fig. S3) had almost no effect on the concentration of LCMs. Fig. 1a shows that the P25/photocatalytic process achieved degradation ratios of 70.0%, 65.6%, 94.2% and 31.8% towards TPrCB, DPrCB, BBDB and ECTB within 60 min, respectively. Their reaction kinetics was studied according to the pseudo-first-order kinetics formula:

$$-\ln(C/C_0) = k_{obs} \times t \quad (2)$$

where k_{obs} is the observed pseudo-first-order rate constant; t is the reaction time; C and C_0 represent the concentration of LCMs at a certain reaction time and the initial concentration of LCMs, respectively [30]. The observed degradation rate constant of BBDB in the P25/photocatalytic process was 0.044 min^{-1} , which was 3.0, 2.6 and 6.8 times to that of DPrCB, TPrCB and ECTB, respectively (Fig. S4).

Based on the concentration of F^- released from the fluorinated LCMs into the aqueous solution in the P25/photocatalytic process, the defluorination ratio (*deF%*) is defined according to the following formula:

Table 1
The molecular structures, ESP and ALIE distributions of LCMs, calculated at B3LYP/6–31G** Level of Theory.

	Molecular formula	M. W.(g mol ⁻¹)	Structure	ESP		ALIE
				-1e-3 a.u. to 1e-3 a.u.		
				● C ● H ● O ● F		
DPrCB	C ₂₁ H ₃₀ F ₂	320.47				
TPrCB	C ₂₁ H ₂₉ F ₃	338.46				
BBDB	C ₂₂ H ₃₀ F ₂	332.48				
ECTB	C ₂₁ H ₂₉ F ₃ O	354.46				

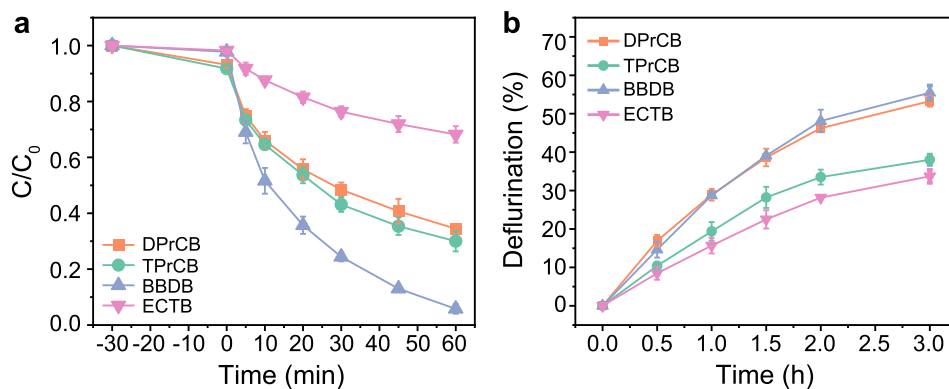


Fig. 1. Degradation (a) and defluorination (b) processes of DPrCB, TPrCB, BBDB and ECTB in the P25/photocatalytic process. Photocatalytic experiments conditions: [LCMs] = 20 mg L⁻¹, [P25] = 0.6 g L⁻¹, pH 6.6.

$$deF\% = \frac{C_{F^-}}{C_0 \times N_{C-F}} \times 100\% \quad (3)$$

where C_0 and C_{F^-} represent the molar concentration of F⁻ released in the solution and the initial molar concentration of LCMs, respectively; N_{C-F} is the number of C–F bonds in the LCMs molecules [31]. As shown in Fig. 1b, the highest $deF\%$ within 3 h was 55.5% for BBDB, followed by DPrCB (53.3%), TPrCB (38.0%) and ECTB (33.7%). The observed defluorination rate constant of BBDB in the P25/photocatalytic process was 0.279 h⁻¹, which was 1.1, 1.7 and 2.0 times higher than that of DPrCB, TPrCB and ECTB, respectively (Fig. S5).

Note that the “degradation” of a parent LCMs requires only one bond to be cleaved, while the “defluorination” needs the C–F bond with higher bond energy to be cleaved. In the same oxidation condition, the cleavages of C–C and C–O are easier to occur due to their lower bond energy in comparison with C–F [31], which result in the degradation rate of the LCMs to be higher than their defluorination rate. Moreover, the defluorination rates of BBDB and DPrCB with two C–F bonds in their molecular structures were much higher relative to TPrCB and ECTB with three C–F bonds, which may be due to the existence of three C–F bonds in a more symmetrical structure in TPrCB and ECTB. Thus, it is hypothesized that the different molecular structures of the fluorinated LCMs may

result in the different degradation and defluorination kinetics in the P25/photocatalytic process.

3.2. Different reaction mechanisms of the fluorinated LCMs

Fig. S6 shows that UV irradiation alone or P25 without irradiation cannot produce oxidizing free radicals. As shown in Fig. 2a, the electron paramagnetic resonance (EPR) signals of DMPO- \bullet OH and DMPO- \bullet O₂⁻ indicated that \bullet OH and \bullet O₂⁻ may jointly contributed to the degradation of LCMs [32–35]. To further determine the respective contribution of the reactive oxidation species (ROS) to the oxidation system, EDTA-2Na, TBA and p-BQ were added as hole (h^+), \bullet OH and \bullet O₂⁻ scavengers, respectively [36–38]. Fig. 2b reveals that compared with no scavengers, EDTA-2Na, TBA and p-BQ suppressed BBDB degradation ratios from 94.2% to 12.1%, 31.0% and 53.6% within 60 min, respectively, which indicated the primary role of h^+ in the oxidation system. Similarly, the quencher experiments of DPrCB (Fig. 2c) and TPrCB (Fig. 2d) demonstrated the primary role of h^+ , followed by \bullet OH and \bullet O₂⁻. Thus, the reaction paths of ROS in the P25/photocatalytic process were proposed as eq. (4)–(6) [39,40]:



Surprisingly, the influences of EDTA-2Na and TBA on the photodegradation of ECTB were very close, which suppressed ECTB degradation ratios from 31.8% to 9.3% and 11.1%, respectively (Fig. 2e). Thus, the contributions of h^+ and \bullet OH were almost the same in ECTB degradation, indicating that \bullet OH generated by h^+ was the main ROS, while the direct oxidation of h^+ might have negligible effects. Generally, h^+ is considered as an electrophile that tends to attack electron-rich sites, whereas \bullet OH and \bullet O₂⁻ can attack both electron-rich sites and electron-deficient sites [11,17,41]. Thus, the different ESP distribution of LCMs was calculated to locate the sites for electrophilic and nucleophilic reactions and predict the initial reaction sites on the molecular structures of the fluorinated LCMs.

As shown in Table 1, the blue color illustrates very negative ESP regions, while the red color represents very positive ESP regions on the vdW surface [42]. The integral ESP regions of DPrCB, TPrCB and BBDB are composed of blue and red color, while their benzene rings and F atoms are mainly composed of blue color, indicating the negative ESP regions on the vdW surface of the benzene rings and F atoms, which are vulnerable to electrophilic attack. ECTB are mainly composed of red color, representing the positive ESP regions on the vdW surface of ECTB for nucleophilic attack. Accordingly,

most reaction sites on DPrCB, TPrCB and BBDB are vulnerable to electrophilic attack, while nucleophilic attack tends to happen on ECTB, resulting in the degradation of DPrCB, TPrCB and BBDB by h^+ , \bullet OH and \bullet O₂⁻ and the decomposition of ECTB by only \bullet OH and \bullet O₂⁻, which is consistent with the results of ROS scavenging experiments. Moreover, the direct oxidation of h^+ in photocatalysis mainly occurs on the surface of photocatalysts. The low adsorption of ECTB by P25 (Fig. 1a) could be another reason for the low contribution of direct h^+ oxidation in ECTB degradation. Generally, the negative ESP regions with smaller ALIE values are more prone to electrophilic attack by h^+ , \bullet OH and \bullet O₂⁻. As shown in Table 1, in the case of DPrCB, TPrCB and BBDB, the areas around the benzene ring and carbon chain possess smaller ALIE values for electrophilic reaction, which corresponds to the local minima of ESP regions marked with darker blue. Thus, the benzene ring opening reaction and carbon chain cleavage might be the initial reaction in the degradation process of DPrCB, TPrCB and BBDB. Moreover, the DD values ($f_A^{(2)}$) of the benzene rings in BBDB, DPrCB and TPrCB are obviously higher than other reaction sites (Table S2–S4), which can further confirm the initial reaction of the benzene ring opening. However, the methoxy group connected to the benzene ring of ECTB has an electron donating conjugation effect [43,44], resulting in the decrease of positive ESP regions on the benzene ring. Thus, the methoxy group can reduce the nucleophilic reactivity on the benzene ring, leading to the darker red color of the methoxy group than the benzene ring in the ESP distribution (Table 1), which implies the initial reaction sites are on the methoxy group rather than the benzene ring of ECTB. Therefore, the contribution of h^+ to ECTB was negligible due to its positive ESP distribution, and the vulnerability of the benzene ring of ECTB was reduced due to the presence of a methoxy group, which together led to the significantly decreased degradation efficiency of ECTB in the P25/photocatalytic process.

3.3. Proposed detoxification pathways of the fluorinated LCMs

The chromatograms of DPrCB, TPrCB, BBDB and ECTB obtained by GC-MS (Figs. S7–8) showed that the LCMs peaks kept decreasing throughout the reaction. Meanwhile, other peaks representing the intermediate products appeared and increased as the reaction progressed, indicating the decomposition of LCMs into some intermediate products. The atomically labeled molecular structures of the four LCMs are shown in Fig. S9. The $f_A^{(2)}$ values of atoms on BBDB (Table S2) implied that 13C (-0.156), 15C (0.259), 16C (-0.165) and 18C (0.252) on the benzene ring might be the primary attack sites by h^+ , \bullet OH and \bullet O₂⁻, leading to the fracture of the benzene ring and the defluorination reactions. Moreover, because of the extremely negative surface charge distribution of 22C (-0.510, q N value) and 24C (-0.494, q N value) in Table S2, the parent molecule was more vulnerable to electrophilic attack. Combining the mass spectra of the possible products of BBDB as

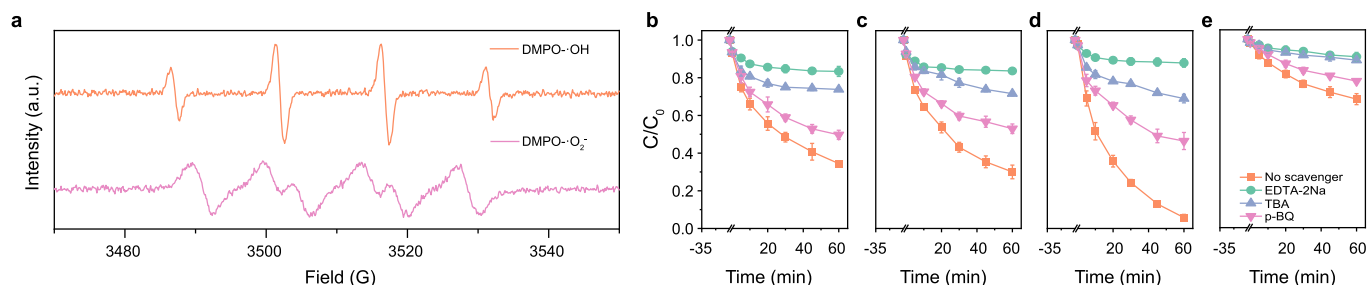


Fig. 2. (a) EPR spectra of DMPO- \bullet OH and DMPO- \bullet O₂⁻ in the P25/photocatalytic process. Effects of various quenching agents on DPrCB (b), TPrCB (c), BBDB (d) and ECTB (e) degradation. Photocatalytic experiments conditions: [LCMs] = 20 mg L⁻¹, [P25] = 0.6 g L⁻¹, pH 6.6. Quenching experiment conditions: [EDTA-2Na] = [TBA] = p-BQ = 1 mM.

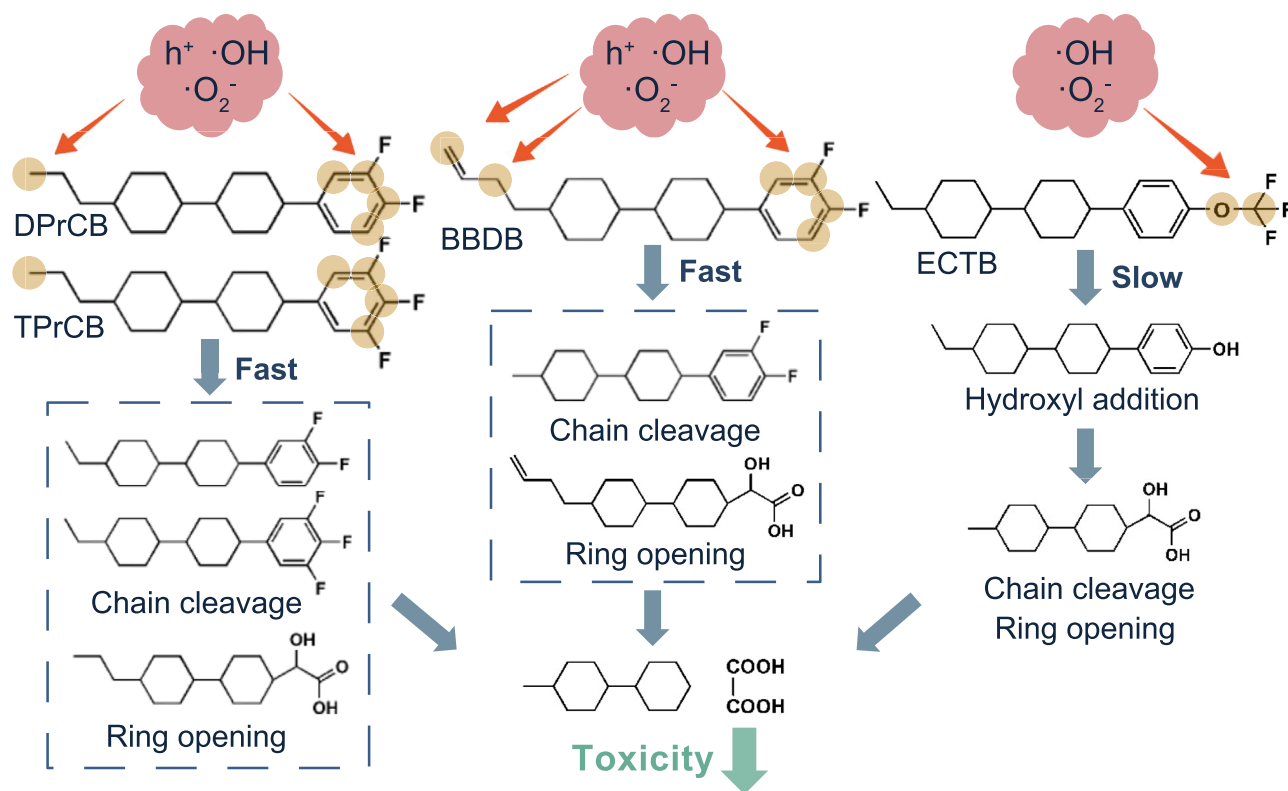


Fig. 3. Schematic illustration of the possible ROS attack mechanisms and detoxification processes of DPrCB, TPrCB, BBDB and ECTB in the photocatalytic processes.

shown in Table S6 and Fig. S10, the inferred potential decomposition pathways of BBDB were two folds, one of which was the cleavage of the carbon chain, and the other was the fracture of the benzene ring (Fig. S11, see SI for detailed description).

To evaluate the environmental impact of LCMs degradation by the P25/photocatalytic process, acute toxicity (oral rat LD_{50}) and developmental toxicity of the photocatalytic degradation products were evaluated by the Toxicity Estimation Software (T.E.S.T.) based on quantitative structure-activity relationship (QSAR) prediction [45–47]. As shown in Fig. S12, the overall toxicity estimation revealed that some LCM intermediates with higher toxicity might be generated through the initial oxidation of the P25/photocatalytic process. Upon further oxidation, some of the highly toxic LCMs intermediates could be decomposed into some final products resulting in a significant reduction in toxicity (see SI for detailed description). The detoxification pathways of ECTB, DPrCB and TPrCB are elaborated in SI.

In summary, the distinct reaction kinetics of the fluorinated LCMs could be attributed to their different degradation mechanisms and detoxification processes following P25/photocatalytic treatment (schematic is shown in Fig. 3). DPrCB, TPrCB and BBDB with mainly negative ESP regions were vulnerable to electrophilic attack by h^+ , $\bullet OH$ and $\bullet O_2^-$, whereas ECTB composed of mainly positive ESP regions were vulnerable to nucleophilic attack by only $\bullet OH$ and $\bullet O_2^-$. The direct oxidation of h^+ could promote the degradation efficiency of LCMs. Moreover, the detoxification processes of DPrCB, TPrCB and BBDB included the cleavage of the carbon chain and benzene ring, resulting in a fast detoxification process generating products with less toxicity. However, the methoxy group of ECTB reduced the nucleophilic reactivity on the benzene ring, leading to a much slower benzene ring opening process and lower detoxification efficiency. The overall toxicity estimation in our work revealed that the typical fluorinated LCMs

with high acute toxicity and developmental toxicity could be decomposed into some final products of significantly less toxicity.

4. Conclusions

In this work, the experimental and theoretical reports of fluorinated LCMs' detoxification processes in the P25/photocatalytic process are provided. The detoxification efficiency of LCMs was strongly influenced by the specific nucleophilic and electrophilic properties of LCMs. BBDB, DPrCB and TPrCB with mainly negative ESP regions were vulnerable to electrophilic attack by h^+ , $\bullet OH$ and $\bullet O_2^-$, while ECTB with mainly positive ESP regions was vulnerable to nucleophilic attack by $\bullet OH$ and $\bullet O_2^-$, which led to a fast detoxification process in BBDB, DPrCB and TPrCB. Inspired by this work, it is possible to perform theoretical calculations and analyses of various LCMs to qualitatively predict whether a certain substitution pattern may impact the detoxification efficiency of LCMs in future work. This approach may provide a theoretical basis for screening candidate photo-degradable LCMs for manufacturing LCDs, and allow for mitigation of the enduring harm of LCMs to the environment.

Conflict of interest

The authors declare no competing financial interest.

Declaration of competing interest

The authors declare that they have no known competing financial interests or personal relationships that could have appeared to influence the work reported in this paper.

Acknowledgements

The present study was financially supported by the Guangdong Basic and Applied Basic Research Foundation (No. 2020B1515020038), the Pearl River Talent Recruitment Program of Guangdong Province (2019QN01L148), the National Natural Science Foundation of China (21876063 and 22076064), the Guangdong Special Support Program (2019TX05L129), the Guangdong (China) Innovative and Entrepreneurial Research Team Program (2016ZT06N258), the Special Fund Project for Science and Technology Innovation Strategy of Guangdong Province (2019B121205004).

Appendix A. Supplementary data

Supplementary data to this article can be found online at <https://doi.org/10.1016/j.ese.2021.100141>.

References

- J. Li, G. Su, R.J. Letcher, W. Xu, M. Yang, Y. Zhang, Liquid crystal monomers (LCMs): a new generation of persistent bioaccumulative and toxic (PBT) compounds? *Environ. Sci. Technol.* 52 (9) (2018) 5005–5006.
- H. Su, S. Shi, M. Zhu, D. Crump, R.J. Letcher, J.P. Giesy, G. Su, Persistent, bioaccumulative, and toxic properties of liquid crystal monomers and their detection in indoor residential dust, *Proc. Natl. Acad. Sci. U.S.A.* 116 (52) (2019) 26450–26458.
- D. Wang, Z. Cai, G. Jiang, A. Leung, M.H. Wong, W.K. Wong, Determination of polybrominated diphenyl ethers in soil and sediment from an electronic waste recycling facility, *Chemosphere* 60 (2005) 810–816.
- Y. Wang, Y. Cao, W. He, G. Li, H. Zhu, J. Huang, The improved treatment of liquid crystals into non-hazardous molecules using a microwave-assisted hydrothermal method, *J. Hazard Mater.* 393 (2020) 122351.
- H. Su, S. Shi, M. Zhu, J. Li, G. Su, Liquid crystal monomers (LCMs) in sediments: method validation and detection in sediment samples from three typical areas, *Environ. Sci. Technol.* 55 (4) (2021) 2336–2345.
- M. Zhu, H. Su, Y. Bao, J. Li, G. Su, Experimental determination of octanol-water partition coefficient (KOW) of 39 liquid crystal monomers (LCMs) by use of the shake-flask method, *Chemosphere* 287 (2022) 132407.
- Q. Liu, J. Liggio, J. Wentzell, P. Lee, K. Li, S.-M. Li, Atmospheric OH oxidation chemistry of particulate liquid crystal monomers: an emerging persistent organic pollutant in air, *Environ. Sci. Technol. Lett.* 7 (9) (2020) 646–652.
- C.J. Woolverton, E. Gustely, L. Li, O.D. Lavrentovich, Liquid crystal effects on bacterial viability, *Liq. Cryst.* 32 (4) (2005) 417–423.
- C. Soriano-Correa, C. Barrientos-Salcedo, M. Francisco-Márquez, C.I. Sainz-Díaz, Computational study of substituent effects on the acidity, toxicity and chemical reactivity of bacteriostatic sulfonamides, *J. Mol. Graph. Model.* 81 (2018) 116–124.
- R. Yin, W. Guo, N. Ren, L. Zeng, M. Zhu, New insight into the substituents affecting the peroxydisulfate nonradical oxidation of sulfonamides in water, *Water Res.* 171 (2020) 115374.
- S. He, R. Yin, T. Lai, Y. Zhao, W. Guo, M. Zhu, Structure-dependent degradation of nitroimidazoles by cobalt-manganese layered double hydroxide catalyzed peroxymonosulfate process, *Chemosphere* 266 (2021) 129006.
- H. Zhao, Y. Zhou, C. Han, Y.D. Liu, R. Zhong, Degradation mechanisms and substituent effects of N-Chloro- α -Amino acids: a computational study, *Environ. Sci. Technol.* 54 (5) (2020) 2635–2645.
- Y. Ji, Y. Fan, K. Liu, D. Kong, J. Lu, Thermo activated persulfate oxidation of antibiotic sulfamethoxazole and structurally related compounds, *Water Res.* 87 (2015) 1–9.
- H. Li, T. Li, S. He, J. Zhou, T. Wang, L. Zhu, Efficient degradation of antibiotics by non-thermal discharge plasma: highlight the impacts of molecular structures and degradation pathways, *Chem. Eng. J.* 395 (2020) 125091.
- Y. Li, Y. Fu, M. Zhu, Green synthesis of 3D tripyramid TiO₂ architectures with assistance of aloe extracts for highly efficient photocatalytic degradation of antibiotic ciprofloxacin, *Appl. Catal. B Environ.* 260 (2020) 118149.
- M. Zhu, P. Chen, M. Liu, Graphene oxide enwrapped Ag/AgX (X = Br, Cl) nanocomposite as a highly efficient visible-light plasmonic photocatalyst, *ACS Nano* 5 (6) (2011) 4529–4536.
- S. He, C. Zhai, M. Fujitsuka, S. Kim, M. Zhu, R. Yin, L. Zeng, T. Majima, Femtosecond time-resolved diffuse reflectance study on facet engineered charge-carrier dynamics in Ag₃PO₄ for antibiotics photodegradation, *Appl. Catal. B Environ.* 281 (2021) 119479.
- S.K. Loeb, P.J. Alvarez, J.A. Brame, E.L. Cates, W. Choi, J. Crittenden, D.D. Dionysiou, Q. Li, G. Li-Puma, X. Quan, The technology horizon for photocatalytic water treatment: sunrise or sunset? *Environ. Sci. Technol.* 53 (6) (2019) 2937–2947.
- D. Xia, H. Liu, B. Xu, Y. Wang, Y. Liao, Y. Huang, L. Ye, C. He, P.K. Wong, R. Qiu, Single Ag atom engineered 3D-MnO₂ porous hollow microspheres for rapid photothermocatalytic inactivation of E. coli under solar light, *Appl. Catal. B Environ.* 245 (2019) 177–189.
- Y. Chen, M. Xu, J. Wen, Y. Wan, Q. Zhao, X. Cao, Y. Ding, Z.L. Wang, H. Li, Z. Bian, Selective recovery of precious metals through photocatalysis, *Nat. Sustain.* 4 (2021) 618–626.
- M. Zhu, M. Shen, X. Liang, H. Chen, C. Zhu, B. Du, D. Luo, S. Lan, Z. Feng, L. Zeng, Identification of environmental liquid-crystal monomers: a class of new persistent organic pollutants—fluorinated biphenyls and analogues—emitted from E-waste dismantling, *Environ. Sci. Technol.* 55 (9) (2021) 5984–5992.
- M. Frisch, G. Trucks, H.B. Schlegel, G.E. Scuseria, M.A. Robb, J.R. Cheeseman, G. Scalmani, V. Barone, B. Mennucci, G. Petersson, Gaussian 09, Revision d. 01, Gaussian, Inc., Wallingford CT 201, 2009.
- R. Yin, W. Guo, H. Wang, J. Du, Q. Wu, J.-S. Chang, N. Ren, Singlet oxygen-dominated peroxydisulfate activation by sludge-derived biochar for sulfamethoxazole degradation through a nonradical oxidation pathway: performance and mechanism, *Chem. Eng. J.* 357 (2019) 589–599.
- C. Li, H.-B. Xie, J. Chen, X. Yang, Y. Zhang, X. Qiao, Predicting gaseous reaction rates of short chain chlorinated paraffins with •OH: overcoming the difficulty in experimental determination, *Environ. Sci. Technol.* 48 (23) (2014) 13808–13816.
- R. Yin, Y. Chen, J. Hu, G. Lu, L. Zeng, W. Choi, M. Zhu, Complexes of Fe (III)-organic pollutants that directly activate Fenton-like processes under visible light, *Appl. Catal. B Environ.* 283 (2021) 119663.
- A.M. Fahim, M.A. Shalaby, M.A. Ibrahim, Microwave-assisted synthesis of novel 5-aminouracil-based compound with DFT calculations, *J. Mol. Struct.* 1194 (2019) 211–226.
- A.M. El-Mahalawy, M.M. Abdou, A.R. Wassel, Structural, spectroscopic and electrical investigations of novel organic thin films bearing push-pull azo-Phenol dye for UV photodetection applications, *Spectrochim. Acta, Part A* 248 (2020) 119243.
- C. Morell, A. Grand, A. Toro-Labbe, New dual descriptor for chemical reactivity, *J. Phys. Chem.* 109 (2005) 205–212.
- R. Yin, W. Guo, J. Du, X. Zhou, H. Zheng, Q. Wu, J. Chang, N. Ren, Heteroatoms doped graphene for catalytic ozonation of sulfamethoxazole by metal-free catalysis: performances and mechanisms, *Chem. Eng. J.* 317 (2017) 632–639.
- Y. Chen, S. Lan, M. Zhu, Construction of piezoelectric BaTiO₃/MoS₂ heterojunction for boosting piezo-activation of peroxymonosulfate, *Chin. Chem. Lett.* 32 (6) (2021), 2052–2056.
- M.J. Bentel, Y. Yu, L. Xu, Z. Li, B.M. Wong, Y. Men, J. Liu, Defluorination of per- and polyfluoroalkyl substances (PFASs) with hydrated electrons: structural dependence and implications to PFAS remediation and management, *Environ. Sci. Technol.* 53 (7) (2019) 3718–3728.
- R. Liu, Y. Xu, B. Chen, Self-assembled nano-FeO (OH)/reduced graphene oxide aerogel as a reusable catalyst for photo-Fenton degradation of phenolic organics, *Environ. Sci. Technol.* 52 (12) (2018) 7043–7053.
- Y. Gao, Y. Zhu, L. Lyu, Q. Zeng, X. Xing, C. Hu, Electronic structure modulation of graphitic carbon nitride by oxygen doping for enhanced catalytic degradation of organic pollutants through peroxymonosulfate activation, *Environ. Sci. Technol.* 52 (24) (2018) 14371–14380.
- D. Xia, W. Xu, Y. Wang, J. Yang, Y. Huang, L. Hu, C. He, D. Shu, D.Y. Leung, Z. Pang, Enhanced performance and conversion pathway for catalytic ozonation of methyl mercaptan on single-atom Ag deposited three-dimensional ordered mesoporous MnO₂, *Environ. Sci. Technol.* 52 (22) (2018) 13399–13409.
- C. He, Y. Wang, Z. Li, Y. Huang, Y. Liao, D. Xia, S. Lee, Facet engineered α -MnO₂ for efficient catalytic ozonation of odor CH₃SH: oxygen vacancy-induced active centers and catalytic mechanism, *Environ. Sci. Technol.* 54 (19) (2020) 12771–12783.
- M. Zhang, J. He, Y. Chen, P.-Y. Liao, Z.-Q. Liu, M. Zhu, Visible light-assisted peroxydisulfate activation via hollow copper tungstate spheres for removal of antibiotic sulfamethoxazole, *Chin. Chem. Lett.* 31 (2020) 2721–2724.
- B. Sun, W. Ma, N. Wang, P. Xu, L. Zhang, B. Wang, H. Zhao, K.-Y.A. Lin, Y. Du, Polyaniline: a new metal-free catalyst for peroxymonosulfate activation with highly efficient and durable removal of organic pollutants, *Environ. Sci. Technol.* 53 (16) (2019) 9771–9780.
- C. He, Y. Liao, C. Chen, D. Xia, Y. Wang, S. Tian, J. Yang, D. Shu, Realizing a redox-robust Ag/MnO₂ catalyst for efficient wet catalytic ozonation of S-VOCs: Promotional role of Ag(0)/Ag(I)-Mn based redox shuttle, *Appl. Catal. B Environ.* 303 (2022) 120881.
- S. Wu, H. Hu, Y. Lin, J. Zhang, Y.H. Hu, Visible light photocatalytic degradation of tetracycline over TiO₂, *Chem. Eng. J.* 382 (2020) 122842.
- X. Hu, X. Hu, Q. Peng, L. Zhou, X. Tan, L. Jiang, C. Tang, H. Wang, S. Liu, Y. Wang, Mechanisms underlying the photocatalytic degradation pathway of ciprofloxacin with heterogeneous TiO₂, *Chem. Eng. J.* 380 (2020) 122366.
- J. Xiao, Y. Xie, Q. Han, H. Cao, Y. Wang, F. Nawaz, F. Duan, Superoxide radical-mediated photocatalytic oxidation of phenolic compounds over Ag⁺/TiO₂: influence of electron donating and withdrawing substituents, *J. Hazard Mater.* 304 (2016) 126–133.
- Y. Tao, X. Li, L. Han, W. Zhang, Z. Liu, Spectroscopy (FT-IR, FT-Raman), hydrogen bonding, electrostatic potential and HOMO-LUMO analysis of toxolone based on DFT calculations, *J. Mol. Struct.* 1121 (2016) 188–195.
- T. Satoh, K. Sumaru, T. Takagi, K. Takai, T. Kanamori, Isomerization of spiropyrans bearing electron-donating and electron-withdrawing groups in acidic aqueous solutions, *Phys. Chem. Chem. Phys.* 13 (2011) 7322–7329.
- X. Meng, L. Wang, Y. Zhai, H. Duan, Electron-donating methoxy group

- enhances the stability and efficiency of indole-based fluorescent probe for detecting Cu^{2+} , Res. Chem. Intermed. 46 (2020) 5517–5533.
- [45] Z. Cai, X. Hao, X. Sun, P. Du, W. Liu, J. Fu, Highly active $\text{WO}_3@$ anatase- SiO_2 aerogel for solar-light-driven phenanthrene degradation: mechanism insight and toxicity assessment, Water Res. 162 (2019) 369–382.
- [46] C. Dang, F. Sun, H. Jiang, T. Huang, W. Liu, X. Chen, H. Ji, Pre-accumulation and in-situ destruction of diclofenac by a photo-regenerable activated carbon fiber supported titanate nanotubes composite material: intermediates, DFT calculation, and ecotoxicity, J. Hazard Mater. 400 (2020) 123225.
- [47] B. Yang, X. Cheng, Y. Zhang, W. Li, J. Wang, H. Guo, Insight into the role of binding interaction in the transformation of tetracycline and toxicity distribution, Environ. Sci. Ecotechnol. 8 (2021) 100127.